Links among warming, carbon and microbial dynamics mediated by soil mineral weathering

S. Doetterl[1,2]*, A. A. Berhe[3], C. Arnold[3], S. Bodé[2], P. Fiener[1], P. Finke[4], L. Fuchslueger[5,6], M. Griepentrog[2,7], J. W. Harden[8,9], E. Nadeu[10], J. Schnecker[6], J. Six[11], S. Trumbore[12], K. Van Oost[10], C. Vogel[13,14] and P. Boeckx[2]

Quantifying soil carbon dynamics is of utmost relevance in the context of global change because soils play an important role in land–atmosphere gas exchange. Our current understanding of both present and future carbon dynamics is limited because we fail to accurately represent soil processes across temporal and spatial scales, partly because of the paucity of data on the relative importance and hierarchical relationships between microbial, geochemical and climatic controls. Here, using observations from a 3,000-kyr-old soil chronosequence preserved in alluvial terrace deposits of the Merced River, California, we show how soil carbon dynamics are driven by the relationship between short-term biotic responses and long-term mineral weathering. We link temperature sensitivity of heterotrophic respiration to biogeochemical soil properties through their relationship with microbial activity and community composition. We found that soil mineralogy, and in particular changes in mineral reactivity and resulting nutrient availability, impacts the response of heterotrophic soil respiration to warming by altering carbon inputs, carbon stabilization, microbial community composition and extracellular enzyme activity. We demonstrate that biogeochemical alteration of the soil matrix (and not short-term warming) controls the composition of microbial communities and strategies to metabolize nutrients. More specifically, weathering first increases and then reduces nutrient availability and retention, as well as the potential of soils to stabilize carbon.

The potential of soils to sequester carbon (C) can vary greatly depending on soil development and how weathering interacts with biological processes that (re)cycle essential nutrients and elements[1–5]. Because of this complexity, assessing the development of soil C stocks and land–atmosphere exchanges[6–8] remains one of the least constrained components of the terrestrial C cycle[9–11]. This is partially due to differing timescales of the processes involved. On the one hand, gross short-term fluxes of C between soil and atmosphere are dominated by processes involving non-protected C, such as respiration of plant residues, root exudation and rhizodeposition. As a result, many studies focus on short-term greenhouse gas fluxes. Studies on the effects of warming on plants and soils hardly exceed time series longer than years to decades[12–14]. Even shorter (years at maximum) are studies that focus on the interactions of microorganisms with the soil mineral matrix. On the other hand, the majority of C stored in soils persists and cycles within soils for decades to millennia, mainly through interactions with secondary soil minerals[15] that are driven by mineral weathering operating on longer timescales[16]. While the importance of the mineral matrix for C stabilization is recognized[3], the links between short-term processes determining the C exchange between land and atmosphere and long-term processes involved in soil genesis are not well studied.

On a chronosequence of felsic, granitic river terrace landforms covered by natural grassland and ranging in age since deposition from 0.1 to 3,000 kyr, we studied the co-evolution of biotic,

mineralogical, geochemical and physical processes in the main rooting zone (0–15 cm depth) of soils. This chronosequence constitutes a space-for-time substitution to observe variability in soil development, across trajectories of soil mineral transformation (from primary to secondary minerals) that were developed under similar conditions (that is, semiarid climate, grassland vegetation, parent material of similar origin), but experienced different duration and intensity of mineral weathering. By combining temperature sensitivity of the specific potential heterotrophic soil respiration (SPR, potential maximum of heterotrophic respiration at a specific temperature, normalized to the C content of the respective bulk soil and measured at 60% water holding capacity) with biogeochemical soil properties, soil microbial activity and community composition, we constrained the magnitude of change in soil C turnover, stocks and temperature sensitivity resulting from mineral transformation along this chronosequence (more information on the experimental approach can be found in Supplementary Section 1.1 and Supplementary Fig. 2).

Weathering effects on C cycling and microbial communities

Along the 3,000 kyr chronosequence, aboveground net primary productivity (ANPP) and root biomass C decreased by about 35% and more than 50%, respectively, with terrace age (Table 1). However, this decrease is nonlinear: ANPP and root biomass C begin to decrease on older terraces only after reaching a

[1]Institute of Geography, Augsburg University, Augsburg, Germany. [2]Isotope Bioscience Laboratory (ISOFYS), Ghent University, Gent, Belgium. [3]School of Natural Sciences Sciences, University of California at Merced, Merced, CA, USA. [4]Department of Environment, Ghent University, Gent, Belgium. [5]Plants and Ecosystems Research Center, Antwerp University, Antwerpen, Belgium. [6]Department of Microbiology and Ecosystem Science, University of Vienna, Vienna, Austria. [7]Department of Earth Sciences, ETH Zurich, Zurich, Switzerland. [8]Soil Biogeochemistry Research Group, Emeritus US Geological Survey, Menlo Park, CA, USA. [9]School of Earth, Energy and Environmental Sciences, Stanford University, Stanford, CA, USA. [10]Earth and Life Institute, Catholic University of Louvain, Louvain-la-Neuve, Belgium. [11]Department of Environmental Systems Science, ETH Zurich, Zürich, Switzerland. [12]Institute for Biogeochemistry, Max Planck Society, Munich, Germany. [13]Institute of Soil Science and Site Ecology, TU Dresden, Dresden, Germany. [14]Research Department Ecology and Ecosystem Management, TU München, Munich, Germany. *e-mail: doetterl@geo.uni-augsburg.de

Table 1 | Overview of soil fertility and biomass production dynamics as a function of soil age through weathering

Terrace age (kyr)	ANPP (g C m^{-2} yr^{-1})	Root biomass (g C m^{-2})	SSA (m^2 g^{-1})	C coverage of MS (%)	Total C (kg m^{-2})	Total N (kg m^{-2})	Total P (kg m^{-2})	CEC$_{pot}$ (cmol$^+$ kg^{-1})	pH (CaCl$_2$)	Bulk density (g cm^{-3})	Gravel (>2 mm) (%)
0.1	100.2 ± 0.8	205.5	8.1 ± 0.02	65	4.6 ± 0.4	0.4 ± 0.14	0.22	15.2	6.8	1.3 ± 0.01	5.8 ± 2.9
3	85.6 ± 12.7	186.0	30.3 ± 0.19	58	6.6 ± 0.6	0.6 ± 0.11	0.14	13.4	6.6	1.21 ± 0.04	7.6 ± 4.1
35	86.3 ± 10.0	268.5	26.7 ± 0.07	26	4.7 ± 1.8	0.4 ± 0.10	0.11	20.8	5.9	1.28 ± 0.02	7.6 ± 2.8
300	80.1 ± 5.6	165.0	4.3 ± 0.11	46	3.2 ± 0.7	0.3 ± 0.10	0.07	4.6	6.1	1.65 ± 0.14	7.9 ± 7.8
3,000	65.7 ± 0.1	103.5	9.0 ± 0.12	36	1.6 ± 0.5	0.2 ± 0.07	0.09	4.5	4.7	1.62 ± 0.06	42.6 ± 3.9

Sampled soil depth 0–15 cm; see Supplementary Information for subsoil information. ANPP, SSA, bulk density and gravel are mean ± s.d. Total C, N and P are average total (organic) carbon (C) (mean ± s.d.), nitrogen (N) (mean ± s.d.) and phosphorus (P). MS, mineral surfaces. For P, pH and CEC$_{pot}$, deviations among duplicate measurements were consistently <5%.

maximum peak in root C productivity at the 3 kyr and 35 kyr terraces, where soil fertility, indicated by potential cation exchange capacity (CEC$_{pot}$), and mineral specific surface area (SSA) are highest. To explain this nonlinearity, we must understand the dynamic shift from a nutrient-abundant to a nutrient-limited system. Primary minerals provide key nutrients to biota; whereas secondary minerals can not only stabilize organic molecules and nutrients for later release, but also enable soil aggregation that occludes nutrients from plant or microbial availability[17,18]. On young terraces (0.1–3 kyr), nutrients are readily released from primary minerals through weathering. At intermediate weathering stages (35 kyr), primary minerals continue to weather, thereby depleting the soil nutrient reserve and decreasing the importance of primary minerals as a source of soil fertility. However, weathering produces highly reactive, clay-sized secondary minerals such as expandable smectite and vermiculite clays that are capable of stabilizing nutrients[16] due to a large increase of SSA compared with their parent minerals, hence reducing nutrient losses through leaching. Both stages provide suitable conditions for plant growth and high C input, where nutrients are still abundant and readily available. As weathering continues to alter secondary minerals, it creates less reactive minerals such as non-expandable kaolinite and halloysite clays, less capable of releasing and/or stabilizing nutrients in soils. Importantly, we also observed a strong decrease of aggregation with terrace age, thereby suggesting a decrease in potential soil C stabilization with soil age (Fig. 1a,b and Table 1). Carbon density in the main rooting zone (0–15 cm soil depth) decreased fourfold, peaking at the 3 kyr terrace (6.6 ± 0.6 kg C m^{-2}) and being lowest at the 3,000 kyr terrace (1.6 ± 0.5 kg C m^{-2}). A large part of this decrease in C density was related to decreases in unprotected, plant-derived C (that is, coarse particulate organic matter) and C in aggregates (physically protected C), while C associated with finer soil particles (C predominantly protected by organo–mineral interaction) was less affected (Fig. 1a; a more detailed discussion on weathering and stabilization mechanisms can be found in Supplementary Section 1.2). Thus, on older terraces (300–3,000 kyr), a soil environment similar to what is commonly observed in deeply weathered systems all over the world was created[5,19], leading to sharp decreases in soil fertility as indicated by decreasing CEC and C stabilization potential as indicated by lower SSA and aggregation potential (Table 1 and Fig. 1). As low soil fertility limits plant growth and thereby C input, C stocks are not only lower due to less C stabilization but also due to less C input (see Supplementary Sections 1.3 & 1.4 for details and discussion on mechanisms of geochemical soil alterations; Supplementary Fig. 4).

Notably, the shift from a nutrient-abundant to nutrient-limited system is not only reflected in the trajectory of ANPP and root biomass C, but also in adaptations of microbial communities[20]. For example, we observed a significant increase of amino sugar ratios (glucosamine/galactosamine (GlcN/GalN)) at the oldest 3,000 kyr

terrace, reflecting a restructuring of microbial communities from bacteria-dominated to fungi-dominated[21,22] communities, even though the exact direction of this shift is debated[23,24] (Fig. 2a). Numerous studies indicate lower C source availability and quality stimulate the development of a microbial community that is dominated with niche specialists[25,26]. Hence, it is reasonable that we found a fungi-dominated community at the oldest terrace that is equipped with strategies to produce extracellular enzymes to degrade more complex organic matter and able to function in more acidic environments[27–29] (see Supplementary Section 1.5 for more discussion on the interpretation of amino sugars). Furthermore, microbial acquisition strategies through extracellular enzymes along the chronosequence shift from C towards N and P mining with age (Fig. 2b). We argue that the decreases in C:N and C:P acquisition ratios reflect primarily a change in substrate quality as

Fig. 1 | C stocks and key mineralogical parameters in soils in response to weathering. a, Distribution of soil C density among fractions. Unprotected, coarse particulate organic matter, not associated with minerals; mAgg, microaggregate-associated C; s + c, non-aggregated silt and clay-associated C. Error bars represent standard deviation. **b**, Fe$_{total}$/Fe$_{DCB}$ ratios and total Al, Fe and Mn content as measure of weathering degree along the sequence including percentage of low-activity (end member) clays to total clay fraction. Deviations among replicate measurements of Fe$_{total}$/Fe$_{DCB}$ ratios <5%. All displayed soil parameters are for the 0–15 cm depth increment; for more information on weathering indexes and fractions, see the Supplementary Information and Methods.
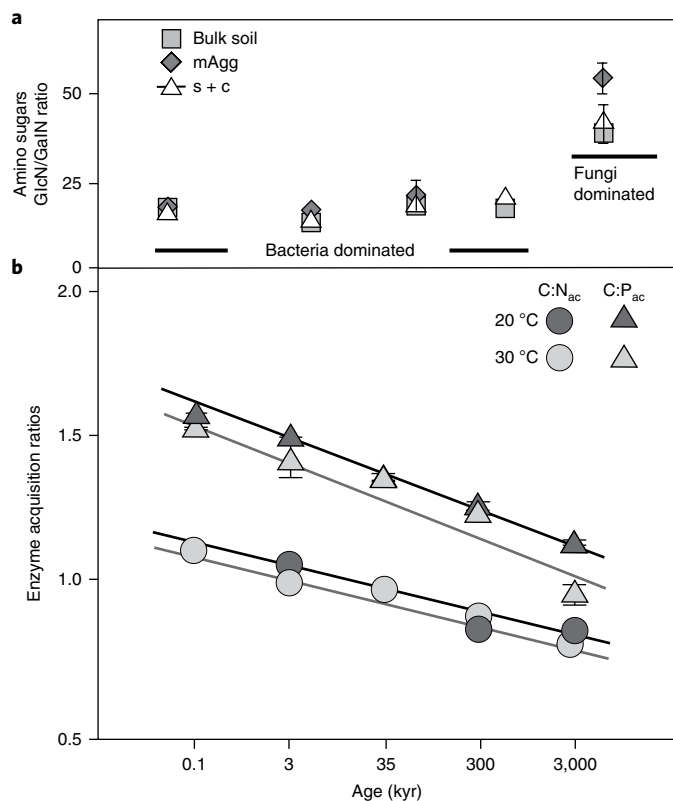
Fig. 2 | Response of microbial community composition and nutrient mining to weathering. a, GlcN/GalN ratio as an indicator for fungi-dominated to bacteria-dominated microbial communities. **b**, C:N and C:P acquisition (ac) ratios of enzymes after 60 d incubation at 20 °C and 30 °C (mean ± s.d.; $n = 3$). Lines (black, 20 °C; grey, 30 °C) indicate statistically significant relations ($P > 0.05$) between soil age and acquisition ratios. All displayed parameters are for the 0–15 cm depth increment.

Fig. 3 | Temperature sensitivity and C fluxes of bulk soil and fractions in response to weathering. a, SPR at 20 °C and Q_{10} (30/20 °C) for bulk soil and mineral-associated fractions. Error bars indicate s.d. of SPR and colours indicate the respective Q_{10} per fraction. **b**, Radiocarbon content (pM-^{14}C) of bulk soil, microaggregate-associated C and free silt and clay-associated C, and respired CO_2 at 20 °C (blue circles) and 30 °C (red circles). Average error in pM-^{14}C measurements: 0.43%. All displayed parameters are for the 0–15 cm depth increment.

P and N become increasingly limited[30]. These C:P and C:N shifts are consistent with a decreasing importance of plant material as a nutrient source for heterotrophic microorganisms towards an increasing importance of recycled microbial residues in older soils; the latter is supported by C radioisotope data (Supplementary Table 4) and indicated by relative increases in N-acetylglucosaminidase kinase activity (an enzyme that mines key components of microbial cell walls). The growing importance of nutrient recycling in older soils is further supported by decreasing fresh plant C inputs with terrace age (Table 1) leading to a general decrease of percent modern carbon (pM-^{14}C) and slower C turnover in soils (Fig. 3b).

Interplay of weathering and warming for soil respiration

The SPR increased by ca. 37% for the bulk soil, 34% for the silt and clay-associated fractions and by more than 66% for the aggregated C with age along the sequence. While no significant difference in temperature sensitivity of SPR (expressed as Q_{10}) was observed for the bulk soil ($Q_{10} = 1.9 \pm 0.2$) along the chronosequence, Q_{10} of SPR for C associated with soil aggregates decreased by almost 60%, limiting the effect of warming-related C release on older terraces (Fig. 3a and Supplementary Table 6). Remarkably, no statistically significant difference in enzyme activity rates at 20 °C compared with 30 °C incubation temperature were observed, indicating that differences in acquisition strategies in soil are more strongly tied to changing soil properties due to weathering (and may include long-term adaptation to climate) than to short-term temperature conditions (Fig. 2b). Noteworthy, the absolute activity of enzymes

at 20 °C compared with 30 °C averaged over all measured enzymes (see Methods) was also not significantly different (data not shown). Comparing the radiocarbon content of bulk soil to that of respired CO_2 revealed that respired CO_2 of younger (0.1–3 kyr) terraces was not significantly different from that of the bulk soil, with no significant difference between the 20 °C and 30 °C incubation experiments. The radiocarbon content of CO_2 respired from 35 kyr terrace soil, however, was significantly lower than that of bulk soil for the 20 °C incubation (−1 to −7% pM^{14}C in CO_2 versus soil). Older terraces (300–3,000 kyr) showed a different response: radiocarbon content of CO_2 was generally higher compared with bulk soil (+12 to +7 pM^{14}C in CO_2 versus soil), again with no significant difference between the 20 °C and 30 °C incubation experiments (Fig. 3b). This pattern indicates that terrace age affected the uptake and respiration of old C versus young C, but incubation temperature did not. With increasing terrace age, microbial respiration is discriminating against older C sources. A possible explanation for this discriminative respiration could be the fast incorporation and mineralization of new C into microbial biomass while older mineral-associated C remains largely untouched due to higher energetic barriers that cannot be overcome in old, nutrient-poor soils[31], with organic matter of predominately microbial origin stabilized with minerals[11,12,32]. However, while there might be an effect of (bio)chemical structure and age of C molecules on the isotopic signature of respired C (Fig. 3b), it is not as an important mechanism to explain C stabilization or release in these soils compared with aggregation or mineral association of C (Fig. 3a).

From our findings along the chronosequence, we draw several overarching conclusions (Fig. 4a). The progression of mineral weathering affects all compartments of the soil C cycle, with control over C inputs and loss, as well as persistence and temperature
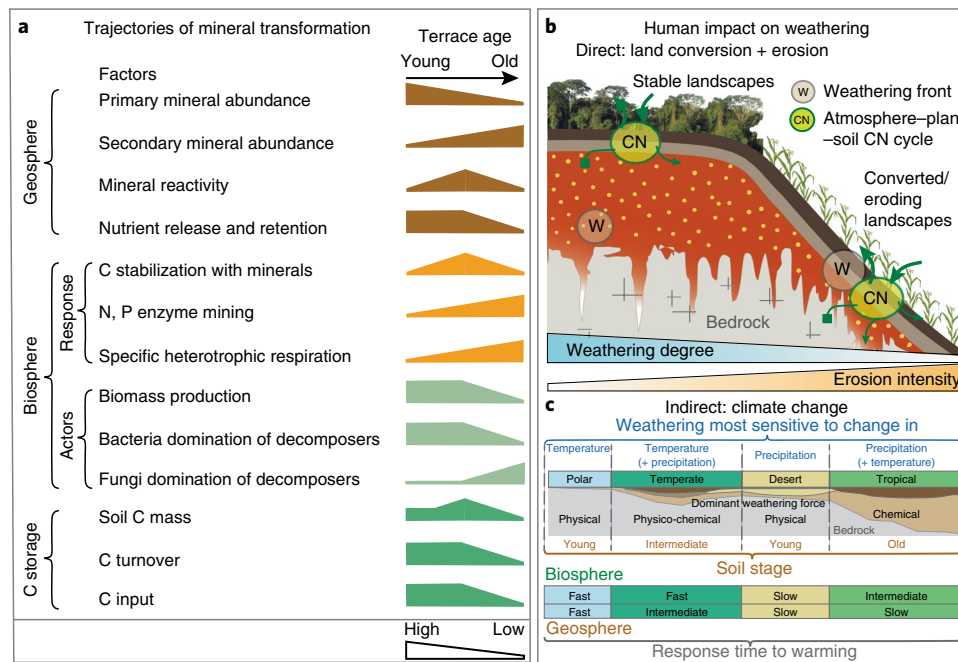
Fig. 4 | Trajectories of mineral transformations and the link to human impact on weathering. a, Conceptual schematic overview of the main changes along the terrace sequence to the geosphere related to weathering as well as response and importance of different processes in the biosphere on C dynamics (conceptualized following the statistically significant ($P < 0.05$) trends of the field-based data along the chronosequence). **b,c,** These trajectories can be found and applied in various geomorphic and geo-climatic settings: along eroding hillslopes, where human activity can influence the degree of soil formation by removing the most weathered soil material through erosion, bringing the weathering front close to the surface (where CNP cycling is taking place and exchange of these elements with plants and atmosphere (arrows) is heavily influenced by the mineral matrix, **b**); or across climate zones, where soil weathering has reached different degrees of intensity, and climatic changes can trigger a variety of CNP cycle responses in soils depending on prior conditions of soil formation and the prevailing climatic barriers to weathering and plant growth (**c**).

sensitivity of soil C. Carbon stocks in soils decrease due to lower C inputs as a result of changes in soil fertility but also due to reduced capacity of soil minerals to stabilize and retain C. While microbial physiology directly controls the response of soil C storage and turnover to warming[33], microbial communities and their acquisition strategies for C, N or P are governed by availability and accessibility of these elements, which is controlled by soil weathering[34]. Thus, weathering diversifies the microbial response to warming (Fig. 3 and Supplementary Table 5) and decomposer communities as a whole adapt well to this wide range of geochemical soil conditions[35]. Furthermore, the rates at which extracellular enzymes are contributing to nutrient mining were affected by the age of the terrace sediment and the soils developed on them, but not by incubation temperature. Hence, in our study of a wide range of geochemically different soils under similar land use, vegetation and climate, C storage was predominantly controlled by long-term weathering processes. From a conceptual point of view, the limitation and potential of soils to sequester C is input driven in soils with limited stabilization capacities (very young and very old soils due to the lack of reactive mineral surfaces, unlike soils of intermediate weathering stages). However, young soils are capable of releasing nutrients in great abundance from primary minerals leading to high plant biomass yields while old soils lack this source of nutrient input (Table 1 and Supplementary Table 2). Decomposer communities simultaneously adjust to a wide range of soil and environmental conditions[36,37]. Importantly, our results show that shorter-term responses of the C cycle, such as changes in respiration or biomass production, are not predictable from initial soil C stock assessments plus warming alone. Older soils are less responsive to warming than younger soils as the latter have generally less reactive, highly weathered minerals (kaolin group clays, chlorites and so on) and the age of soil C is

not necessarily a good indicator for potential stability, hence old C in soils is not more recalcitrant per se[38–40] (more discussion on the weathering-related interplay of capacity and demand for C stabilization along the sequence can be found in Supplementary Section 1.5).

Looking beyond the chronosequence

The geochemistry along this sequence reflects conditions that can be found in major, global geo-climatic ecozones and have the potential to be greatly altered by climate change and human activity (Fig. 4b,c). For mineral soils, the largest potential responses to warming can be expected in the youngest soils that are the least exposed to weathering, as, for example, in higher latitudes. If climatic limitations to chemical weathering would disappear, these areas will see a great change in C cycling within years to decades[41]. Similarly, land conversion and erosion can lead to the removal of weathered material, changing the mineral matrix in which biological processes take place and drastically change the geochemical conditions for C stabilization[42]. Hence, mineral transformation due to weathering impacts the functional link between microbial community structure and soil geochemistry and mediates the soil response to warming as well as C and nutrient dynamics in soils over large spatial and long temporal scales[9,10].

Methods

Methods, including statements of data availability and any associated accession codes and references, are available at https://doi.org/10.1038/s41561-018-0168-7.

References

1. Friedlingstein, P. et al. Uncertainties in CMIP5 climate projections due to carbon cycle feedbacks. *J. Clim.* **27**, 511–526 (2014).
2. Todd-Brown, K. E. O. et al. Causes of variation in soil carbon simulations from CMIP5 Earth system models and comparison with observations. *Biogeosciences* **10**, 1717–1736 (2013).
3. Doetterl, S. et al. Soil carbon storage controlled by interactions between geochemistry and climate. *Nat. Geosci.* **8**, 780–783 (2015).
4. Hartmann, J., Moosdrof, N., Lauerwald, R., Hinderer, M. & West, A. J. Global chemical weathering and associated P-release—the role of lithology, temperature and soil properties. *Chem. Geol.* **363**, 145–163 (2014).
5. Lawrence, C. R., Harden, J. W., Xu, X., Schulz, M. S. & Trumbore, S. E. Long-term controls on soil organic carbon with depth and time: a case study from the Cowlitz River Chronosequence, WA USA. *Geoderma* **247–248**, 73–87 (2015).
6. Hicks Pries, C. E., Castanha, C., Porras, R. & Torn, M. S. The whole-soil carbon flux in response to warming. *Science* **355**, 1420–1423 (2017).
7. Lehmann, J. & Kleber, M. The contentious nature of soil organic matter. *Nature* **528**, 60–68 (2015).
8. Davidson, E. A. & Janssens, I. A. Temperature sensitivity of soil carbon decomposition and feedbacks to climate change. *Nature* **440**, 165–173 (2006).
9. Ciais, P. et al. in *Climate Change 2013: The Physical Science Basis* (eds Stocker, T. F. et al.) 465–570 (Cambridge Univ. Press, 2013).
10. Friend, A. D. et al. Carbon residence time dominates uncertainty in terrestrial vegetation responses to future climate and atmospheric CO_2. *Proc. Natl Acad. Sci. USA* **111**, 3280–3285 (2014).
11. Oertel, C., Matschullat, J., Zurba, K., Zimmermann, F. & Erasmi, S. Greenhouse gas emissions from soils—a review. *Geochemistry* **76**, 327–352 (2016).
12. Leblans, N. I. W. et al. Phenological responses of Icelandic subarctic grasslands to short-term and long-term natural soil warming. *Global Change Biol.* **23**, 4932–4945 (2017).
13. Knorr, W., Prentice, I. C., House, J. I. & Holland, E. A. Long-term sensitivity of soil carbon turnover to warming. *Nature* **433**, 298–301 (2005).
14. Frey, S. D., Lee, J., Melillo, J. M. & Six, J. The temperature response of soil microbial efficiency and its feedback to climate. *Nat. Clim. Change* **3**, 395–398 (2013).
15. Cotrufo, M. F. et al. Formation of soil organic matter via biochemical and physical pathways of litter mass loss. *Nat. Geosci.* **8**, 776–779 (2015).
16. Opolot, E. & Finke, P. A. Evaluating sensitivity of silicate mineral dissolution rates to physical weathering using a soil evolution model (SoilGen2.25). *Biogeosciences* **12**, 6791–6808 (2015).
17. Barré, P., Fernandez-Ugalde, O., Virto, I., Velde, B. & Chenu, C. Impact of phyllosilicate mineralogy on organic carbon stabilization in soils: incomplete knowledge and exciting prospects. *Geoderma* **235–236**, 382–395 (2014).
18. Vitousek, P. M. & Chadwick, O. A. Pedogenic thresholds and soil process domains in basalt-derived soils. *Ecosystems* **16**, 1379–1395 (2013).
19. Six, J., Conant, R. T., Paul, E. & Paustian, K. Stabilization mechanisms of soil organic matter: implications for C-saturation of soils. *Plant Soil* **241**, 155–176 (2002).
20. Moore, J., Macalady, J. L., Schulz, M. S., White, A. F. & Brantley, S. L. Shifting microbial community structure across a marine terrace grassland chronosequence, Santa Cruz, California. *Soil Biol. Biochem* **42**, 21–31 (2010).
21. Griepentrog, M. et al. Nitrogen deposition promotes the production of new fungal residues but retards the decomposition of old residues in forest soil fractions. *Global Change Biol.* **20**, 327–340 (2014).
22. Bodé, S., Fancy, R. & Boeckx, P. Stable isotope probing of amino sugars—a promising tool to assess microbial interactions in soils. *Rapid Commun. Mass Spectrom.* **27**, 1367–1379 (2013).
23. Bai, Z., Bodé, S., Huygens, D., Zhang, X. & Boeckx, P. Kinetics of amino sugar formation from organic residues of different quality. *Soil Biol. Biochem.* **57**, 814–821 (2013).
24. Engelking, B., Flessa, H. & Joergensen, R. G. Shifts in amino sugar and ergosterol contents after addition of sucrose and cellulose to soil. *Soil Biol. Biochem.* **39**, 2111–2118 (2007).
25. Fabian, J., Zlatanovic, S., Mutz, M. & Premke, K. Fungal–bacterial dynamics and their contribution to terrigenous carbon turnover in relation to organic matter quality. *ISME J.* **11**, 415–425 (2017).
26. Monard, C., Gantner, S., Bertilsson, S., Hallin, S. & Stenlid, J. Habitat generalists and specialists in microbial communities across a terrestrial–freshwater gradient. *Sci. Rep.* **6**, 37719 (2016).
27. de Graaff, M. A., Classen, A. T., Castro, H. F. & Schadt, C. W. Labile soil carbon inputs mediate the soil microbial community composition and plant residue decomposition rates. *New Phytol.* **188**, 1055–1064 (2010).
28. de Vries, F. T. et al. Extensive management promotes plant and microbial nitrogen retention in temperate grassland. *PLoS ONE* **7**, e51201 (2012).
29. Wardle, D. A. et al. Ecological linkages between aboveground and belowground biota. *Science* **304**, 1629–1633 (2004).
30. Sinsabaugh, R. L. & Shah, J. J. F. Ecoenzymatic stoichiometry of recalcitrant organic matter decomposition: the growth rate hypothesis in reverse. *Biogeochemistry* **102**, 31–43 (2011).
31. Barré, P. et al. The energetic and chemical signatures of persistent soil organic matter. *Biogeochemistry* **130**, 1–12 (2016).
32. Liang, C., Schimel, J. P. & Jastrow, J. D. The importance of anabolism in microbial control over soil carbon storage. *Nat. Microbiol.* **2**, 17105 (2017).
33. Allison, S. D., Wallenstein, M. D. & Bradford, M. A. Soil-carbon response to warming dependent on microbial physiology. *Nat. Geosci.* **3**, 336–340 (2010).
34. Turner, S. et al. Mineralogical impact on long-term patterns of soil nitrogen and phosphorus enzyme activities. *Soil Biol. Biochem.* **68**, 31–43 (2014).
35. Sinsabaugh, R. L., Hill, B. H. & Shah, J. J. F. Ecoenzymatic stoichiometry of microbial organic nutrient acquisition in soil and sediment. *Nature* **462**, 795–598 (2009).
36. Birkhofer, K. et al. General relationships between abiotic soil properties and soil biota across spatial scales and different land-use types. *PLoS ONE* **7**, e43292 (2012).
37. Fierer, N., Brafdorf, M. A. & Jackson, R. B. Towards an ecological classification of soil bacteria. *Ecology* **88**, 1354–1364 (2007).
38. Dungait, J. A., Hopkins, D. W., Gregory, A. S. & Whitmore, A. P. Soil organic matter turnover is governed by accessibility not recalcitrance. *Global Change Biol.* **18**, 1781–1796 (2012).
39. Sierra, C. A., Müller, M., Metzler, H., Manzoni, S. & Trumbore, S. E. The muddle of ages, turnover, transit, and residence times in the carbon cycle. *Global Change Biol.* **23**, 1763–1773 (2017).
40. Bradford, M. A. et al. Managing uncertainty in soil carbon feedbacks to climate change. *Nat. Clim. Change* **6**, 751–758 (2016).
41. Sistla, S. A. et al. Long-term warmin restructures Arctic tundra without changing net soil carbon storage. *Nature* **497**, 615–618 (2013).
42. Doetterl, S. et al. Erosion, deposition and soil C: a review of process-level controls, experimental tools and models to address C cycling in dynamic landscapes. *Earth Sci. Rev.* **154**, 102–122 (2016).

Author contributions

S.D. and A.A.B. designed the research and co-authors are listed in alphabetical order. S.D., A.A.B., J.Six, K.V.O. and J.W.H. conducted sampling campaigns. S.D., C.A., L.F., J.Schnecker, J.Six, C.V., E.N. and M.G. collected, analysed and interpreted the data. All authors contributed to the writing of the paper.

Competing interests

The authors declare no competing interests.

Additional information

Publisher's note: Springer Nature remains neutral with regard to jurisdictional claims in published maps and institutional affiliations.

Methods

Study site selection and sampling. Soil samples were taken in December 2013 from rangeland under extensive land use along a sequence of alluvial terrace deposits of the Merced River in the Californian Central Valley (Merced County, CA, USA) (Supplementary Fig. 1 and Supplementary Table 1). Our sites are located on the terraces east of the Merced River across an area of about 25×25 km distance. Soil profile descriptions were done using the Food and Agriculture Organization (FAO) guidelines[43] and classified using the World Reference Base for Soil Resources (WRB)[44]. Partly, this campaign resampled terraces and sites where legacy data on soil mineralogy and geochemistry was available[45–50]. Where new sites have been selected, ratios of Ti/Zr and Fe_{total}/Fe_{DCB} have been measured as indicators for the weathering stage of the deposits and compared with the existing mineralogical data to constrain the placement of the selected sites along the timeline of the terrace sequence. The deposits consist of felsic, magmatic and metamorphic material of similar geochemistry and of fine sandy and silty texture, mobilized in the Sierra Nevada mountain range[45]. While no consistent changes are detectable among the fine soil texture, an increase of coarse fragments (quartz pebbles) has been observed in the oldest terrace (Supplementary Table 1). The terrace sequence is situated under the typical semiarid climate of the Californian Central Valley with long-term climate data indicating a relatively climatic similarity (that is, the same Köppen climate class, but fluctuations in mean annual temperature (MAT) and mean annual precipitation (MAP)) for the time period covered by the terrace sequence and very strong climatic similarity over the course of the Holocene with no major fluctuations in MAT and MAP[51,52] (Köppen, BSk; MAT, 16.3 °C; MAP, 315 mm). While the terraces are mostly flat, plateau-like structures, the incision of the Merced River has created noteworthy altitudinal differences from the oldest ($\approx$220 m above sea level) to the youngest ($\approx$50 m above sea level) terrace, with the youngest terrace being geochemically equivalent to the actual modern alluvial terrace and riverbed of the Merced River. Note that none of the investigated terraces is influenced by ground water or stream water dynamics. The lowest terrace is situated in a dry valley, created by an accidental flash flood resulting from the breach of a nearby water reservoir in 1914. For five different terraces, covering the complete temporal range of the terrace sequence (0.1–3,000 kyr), 1 m³ sized soil profiles were excavated covering dystric Fluvisols (youngest terrace) and chromic Alisols (other terraces). At each terrace, from three replicate soil profiles, soil samples were taken from the main rooting zone of soil (topsoil 0–15 cm). After sampling, soils were dried at 40 °C, homogenized and sieved at 2 mm with roots >2 mm removed. Data on biogeochemical soil variables are available for C-deprived subsoil (>15 cm) in the Supplementary Information for context and further discussion. Where not described differently, all follow-up laboratory experiments and extractions are reported as the mean of three replicates.

Aboveground net primary productivity (ANPP) and root C biomass. The dominant vegetation for most of the period of soil formation at the study sites are remnants of the Californian Central Valley perennial bunchgrass ecosystems with no major differences in species composition and dominance. Today's vegetation is now mainly European annual grasses. ANPP for the study region has been estimated based on normalized difference vegetation index (NDVI) data for 2010–2015 according to ref. [53]. Briefly, a five-year average of the integral of the NDVI (NDVI-I) was calibrated and used to derive spatially aggregated values of ANPP. The NDVI averaged for 2010–2015 was derived from the MOD13Q1 Modis (TERRA) vegetation indices 16 d global 250 m product accessed from NASA Land Processes Distributed Active Archive Center at the USGS Earth Resources Observation and Science Center through the Google Earth Engine platform[54]. Carbon biomass of ANPP has been estimated using average reference values from literature for grassland in the study region (45.3 ± 0.2% C)[55]. Root biomass C (g C m^{-2}) was derived from root abundance calculations[56] using dry sieving to isolate >2 mm roots assessed at the time of sampling. Briefly, for each site and soil horizon, fine roots were categorized according to size and abundance and then translated into mg C based on an average of 48% C of the total fine root biomass.

Physical soil parameters and visual observations at profile pits. Soil texture was analysed using a Mastersizer 2000 laser diffraction particle size analyser (Malvern Instruments) and correction factors for the underestimation of clay in silty soils were applied[57,58]. Bulk density was analysed according to ref. [59]. Redoximorphic features have been identified through visually qualifying the relative amount of visible amounts of Fe-Mn nodules, concretions and Fe-reduced areas in soil horizons <1 m during the sampling campaign (Supplementary Table 2).

Geochemical soil parameters. *Elemental composition and degree of weathering.* Total reserve in base cations (the sum of total content in Ca, Na, K, Mg, in cmol$_c$ kg^{-1}) was measured following ref. [60]. Total reserve in base cations can be used to compare soil material of similar depth along the terrace sequence and to evaluate the weathering degree of soil material by assessing the relative loss of Ca, Na, K and Mg cations during weathering. Total elemental content was determined by inductively coupled plasma-atomic emission spectrometry (ICP-AES) on the bulk soil after borate fusion[61]. The same procedure was used to determine the total concentrations of several other elements such as P, Mn, Ti and Zr. An extraction of total pedogenic organo–mineral associations and oxy-hydroxides was carried out in duplicate using dithionite-citrate-bicarbonate (DCB)[62] at pH 8. This allows assessment of the amount of Fe- and Al-bearing phases that have formed through pedogenesis. DCB extractable components were analysed for Al and Fe content by ICP-AES. In addition, the degree of soil weathering was estimated by comparing the ratios of Ti/Zr and Fe_{total}/Fe_{DCB} with Ti and Fe_{DCB} enriching over time relative to the Zr and Fe_{total} content, respectively[45].

pH, CEC and base saturation. Soil pH values were determined as the mean of two measurements per sample after a response time of 30 min and 24 h, respectively, in a 1:2.5 soil (weight)/solution (volume) ratio in 25 ml of 0.01 M $CaCl_2$ potentiometrically with a glass electrode using a portable multiparameter Meter HI9828 (Hanna Instruments). CEC_{pot} was determined by quantifying NH_4^+ exchanged with 2 M KCl after saturating cation exchange sites with ammonium acetate[63] buffered at pH 7.0. Exchangeable Al was extracted by 1 M KCl solution and determined colorimetrically. The total percent base saturation, defined as the relative availability of all base cation (that is, the sum of all base cations Na, K, Mg, Ca) for CEC_{pot}, was calculated in percent of CEC_{pot}.

Clay mineralogy. The mineralogy of the clay-sized fraction was determined by X-ray diffraction (Cu Kα, D8, Brucker Advance) after K$^+$ and Mg^{2+} saturation, ethylene glycol solvation and thermal treatments at 300 and 550 °C (ref. [64]). Clay minerals were classified and peak-identified according to ref. [65]. Quantitative analyses were performed using the Rietveld method through the software package Siroquant V4.0. Refinement of Rietveld parameters was carried out following the instructions provided in the 'Siroquant V4.0 Technical and Clay Manuals' until a chi-square value < 3 was obtained. Key primary minerals that can interfere with the spectra (quartz) and act as sources for clay formation such as amphiboles (hornblende), feldspars (albite, orthoclase, plagioclase), mica (muscovite, phengite, biotite) as well as olivine and pyroxene have been quantified to analyse their relative abundance in relation to the secondary aluminosilicates. For the secondary aluminosilicates, we focused on the identification of expandable 2:1 layered minerals such as smectite and vermiculite, the non-expandable 2:1 layered illite and chlorite and the non-expandable 1:1 layered kaolinite. Note that no distinction has been made between primary and secondary chlorite. In a final step, secondary clay mineral abundance was compared along the terrace sequence.

Specific surface area (SSA). The SSA of the bulk soil was determined by N$_2$ adsorption (Autosorb-1 analyser, Quantachrome) using the Brunauer–Emmett–Teller (BET) equation[66], which is a standard method for measuring SSA of soils based on physisorption of N$_2$ gas on a sample at 77 K. Soil samples (<2 mm, removing any visible root and coarse particulate organic matter fragments) were measured before and after C removal to assess the degree of C coverage of mineral surfaces (Supplementary Table 2 and Supplementary Section 1.5). C was removed by oxidation with a 10% H_2O_2 solution at room temperature adding H_2O_2 until no reaction was visible any more for 24 h. N$_2$ adsorption was measured in the relative partial pressure range (p/p_0) of 0.05 to 0.3. Samples were outgassed for 14 h under constant helium flow at 40 °C before measurements were carried out. Duplicate analysis carried out to verify the repeatability of the experiment identified <5.7% relative uncertainty among all investigated samples.

Soil carbon fractionation and C dynamics. All samples have shown no reaction when treated with 10% HCl and are considered free of carbonates. Total soil C content is therefore interpreted as soil organic carbon only. A subsample of 80 g was fractionated in triplicate for each soil and depth layer to derive functional C fractions. We used a method based on the conceptual C fraction model proposed by ref. [67] (Supplementary Fig. 3). Briefly, the scheme consists of a series of physical fractionation techniques applied to isolate C fractions, differentiated by stabilization mechanisms (chemical, biochemical and physical), which can also be associated with different turnover times and C stability. Using a microaggregate isolator, C was fractionated into coarse particulate organic matter C (>250 μm), microaggregate-associated C (mAgg 250–53 μm) and non-aggregated silt and clay C (<53 μm) (for more detail see Supplementary Table 3 adnd Supplementary Section 1.7). To better understand the C composition of the different isolated mineral-associated fractions, we analyse the C concentration of a fraction as well as its stable isotopic composition (δ^{13}C) and CN ratio and compare it with the respective bulk soil measurements along the sequence. Bulk C% and N% of soil, root and litter was measured in 1 g ground subsamples using a dry combustion analyser (Variomax CN, Elementar) with a measuring range of 0.2–400 mg g^{-1} soil (absolute C or N mass in sample) and a reproducibility of <0.5% (relative deviation). Recovery rates exceeding 97% and 91% were obtained for the soil mass as well as C and N concentrations, respectively, across all samples.

Temperature-sensitive soil incubation. Three replicate samples of 15 g of bulk soil, as well as isolated mAgg and silt and clay fractions from each study site were incubated at two different temperature levels (20 versus 30 °C) during a 70 d period (including 10 d pre-incubation at 20 °C for both sets) while keeping temperature and moisture (60% soil water holding capacity) constant for the length of the experiment, by adding demineralized water to the samples throughout the length

of the experiment when necessary) (for more detail see Supplementary Table 5 and Supplementary Section 1.8). Incubation data were used to derive the SPR[68], expressed as CO_2-C per unit soil C, at the respective temperature level of the incubation. CO_2 production was analysed as the average SPR over the complete period of the incubation (pre-incubation excluded) measured at day 7, 30 and 60. Furthermore, SPR data were used to calculate the Q_{10} of the heterotrophic soil respiration (that is, the difference in SPR of the same aliquot samples at 20° to 30°C incubation temperature). Note that for incubating isolated fractions, 3 g of sample were mixed with 12 g of C-free silty/fine sandy soil material, representing the mean texture of the bulk soil (see Supplementary Table 1). Each sample was put in a 955.5 ± 1.3 ml sealed mason jar with no further additives. To avoid CO_2 saturation effects influencing microbial decomposition processes, the incubation jars were flushed with fresh air after each measurement. Samples of the gas mixture within the incubation jars were taken periodically every 3 to 7 d throughout the experiment and analysed for CO_2 concentration using a gas chromatograph (Shimadzu GC-14B, Shimadzu Scientific Instruments).

Isotopic composition and percent modern ^{14}C. Using ^{14}C radiocarbon dating, we estimate C turnover of the organic material associated with bulk soil, mAgg and non-aggregated silt and clay fractions along the sequence to study relative differences between soils and fractions. In addition, at the last sampling point for CO_2 at the end of the incubation experiment, gas samples were analysed for ^{14}C (expressed as the percentage of modern C (pM-^{14}C%)) to identify differences in the ^{14}C signature of mineralized C compared with the incubated soil and soil C fractions. We used these relative differences to evaluate (1) the effectiveness of different fractions in stabilizing C against decomposition, (2) to estimate the input of fresh C through litter decomposition and (3) to estimate the resilience of C against mineralization under different temperature regimes. In short, roughly 1 mg C was sealed into an evacuated Pyrex tube and reduced to graphite[69]. Sample preparation backgrounds have been subtracted, based on measurements of ^{14}C-free coal. The radiocarbon signature of the graphite was measured with accelerator mass spectrometry (NEC 0.5MV 1.5SDH-2 AMS system) at the Keck-Carbon Cycle AMS facility at University of California, Irvine (California, USA). Results have been corrected for isotopic fractionation according to the conventions of ref. [69], with $\delta^{13}C$ values measured on the prepared graphite using the AMS spectrometer. Radiocarbon concentrations are given as fractions of a modern oxalic acid standard and conventional radiocarbon age following the conventions of ref. [70]. Parallel to this, all isolated fractions and gas samples were analysed for total C using an elemental analyser (ANCA-GSL PDZ Europa) coupled to an isotope ratio mass spectrometer (IRMS) (2020, SerCon) to investigate $^{13/12}C$ ratios.

Biochemical and microbiological soil properties. *Analysis of amino sugars.* Amino sugar concentrations were determined using liquid chromatography, and were assessed in the bulk soil, as well as for the mineral-associated aggregated (mAgg) and non-aggregated (silt and clay) fractions. Amino sugar extraction and analysis was based on the procedure described by ref. [71]. In brief, samples corresponding to 0.3 mg of N were hydrolysed with 6 M HCl (20ml g^{-1} of sample) at 105°C for 8 h, after which amino sugars were purified on a cationic exchange resin (AG50W-X8, 100–200 Mesh, Hydrogen form, Bio-Rad Lab) before liquid chromatography analysis. The chromatographic separation was performed using a liquid chromatography pump (Surveyor MS-Pump Plus, Thermo Scientific) mounted with a PA20 CarboPac analytical anion-exchange column (3×150 mm, 6.5 µm) and a PA20 guard column (Thermo Scientific), detection was done using IRMS coupled to the liquid chromatography device through an interface (LC-ISOLINK, Thermo Scientific). In soils, only GlcN, GalN, mannosamine and muramic acid are found in quantifiable concentrations. Differences in the GlcN/GalN ratios were interpreted as qualitative changes in microbial community structure with higher ratios indicating a relative shift towards fungal residues and lower ratios a relative shift towards bacterial residues, respectively[23] (for more detail see Supplementary Table 3 and Supplementary Section 1.4). Each sample was extracted in duplicate. Due to the very low contents in muramic acid in the extracts, quantifiable analyses of amino sugars were done for GalN and GlcN only. An analysis of the repeatability between replicated extracts of selected samples shows that the limit for quantifying the investigated amino sugars reliably was 100 and 250 µg amino sugar g^{-1} soil for GalN and GlcN, respectively. Hence, we limit our analysis of amino sugar data to observations that exceed the latter mentioned amino sugar contents and to a description of trends within the dataset.

Potential extracellular enzyme activity rates. Potential enzyme activities were determined fluorimetrically and photometrically using modified microplate assays[72] in soils before (10 d acclimatization at 20°C, 60% water holding capacity) and after incubation for 60 d at 20°C and 30°C, respectively. The assays were conducted with soil aliquots (1 g) suspended in 100 ml of sodium acetate buffer (100 mM, pH 5.5) and ultrasonicated for 1 min. For the fluorometrical enzyme assay, 200 µl of soil suspension were pipetted into black microplates in 5 replicates. Each well received 50 µl of MUF (4-methylumbelliferyl)-labelled substrates: MUF-β-D-cellobioside for cellobiohydrolase (CBH, hydrolytic C mining enzyme), MUF-β-D-glucopyranoside, for β-glucosidase (BG, hydrolytic C mining enzyme)

and MUF-N-acetyl-β-D-glucosaminide for N-acetylglucosaminidase (NAG, hydrolytic N mining enzyme). L-leucine-7-amido-4-methylcoumarin was used as substrate for leucine-amino-peptidase (LAP, hydrolytic N mining enzyme). MUF-phosphate was used for phosphatase activity (PHOS, hydrolytic P mining enzyme). Microplates were then incubated at 20°C and 30°C, respectively, for 140 min. Fluorescence was measured with excitation at 365 nm and emission at 450 nm, activity was quantified against standards of MUF and 7-amido-4-methylcoumarin. Phenoloxidase (POX, oxidative enzyme, mining various nutrients) and peroxidase (PEX, oxidative enzyme, mining various nutrients) activities were determined photometrically using L-3,4-dihydroxyphenyl-L-alanine (DOPA) as substrate. For this assay, triplicates of 1 ml of the soil suspension received 1 ml of a 20 mM DOPA solution. After shaking, samples were centrifuged, followed by pipetting 250 µl into duplicate microplates for POX and PEX determination. To determine PEX activities, one set of plates additionally received 10 µl of 0.3% H_2O_2. Then activity was measured photometrically at an absorbance of 450 nm at the start and after 20 h of incubation at 20°C and 30°C, respectively. POX activity rates were calculated as the difference in absorption over incubation time in the plates without H_2O_2. PEX activity rates were calculated as the difference between the changes over time of POX activities and the activities of the plates with H_2O_2 additions[73]. We tested whether terrace age or incubation temperature affects microbial functioning using enzyme activity rates per unit soil C before and after incubation at 20°C and 30°C. Moreover, we tested whether microbes adjust their nutrient acquisition strategy to different temperatures by calculating nutrient acquisition rates based on potential enzyme activity rates. The C:N acquisition by enzymes was calculated as the sum of log-transformed BG and CBH activities over the sum of log-transformed activities of LAP and NAG at the end of the incubation experiment. Similarly, C:P acquisition was calculated as the sum of log-transformed BG and CBH activities divided by the log-transformed PHOS activity at the end of the incubation experiment[74]. The relative difference along the chronosequence and among the ratios is of great interest for interpreting microbial nutrient acquisition strategies[73–75].

Implementation and statistical analyses. All statistical analysis was realized using SPSS 24.0[76] and R 3.3.2[77]. Differences between the means of classes have been performed using multi-group analysis of variance (ANOVA), Bonferroni corrections, Tukey's honest significant difference test and Tamhane's T2. Linear regressions were done to test correlations between the abundance of the reactive soil phases and C in the bulk soil and for the isolated fractions. In addition, step-wise linear regressions were used to estimate the best prediction model for Q_{10} and SPR at 20°C and 30°C for the bulk soil and fractions using the abiotic, mineralogy-related parameters and C input variables assessed in this study (for more details on these results, see Supplementary Table 6 and Supplementary Section 1.8). These models were tested for the (1) homogeneity of model residues and (2) normality of variables, restricted to (3) models were the variable inflation factor for each variable is <1.5 and where (4) an added variable improves the overall model performance (corrected R^2) by >0.1. All statistical tests used in this study were evaluated using $P < 0.05$ as the level of significance. Please note that throughout the manuscript C mass refers to the C concentration of a sample multiplied by the mass of the fraction it is extracted from or multiplied by the bulk density in case of C mass of the bulk soil. Measured values are normalized to the C content of the respective soil or fraction (that is, amino sugar·soil C^{-1}, CO_2-C·soil C^{-1} and so on) to evaluate the relative differences in the relationship of certain parameters to total C in soil. To test whether soil age, soil depth or incubation temperature affects microbial functioning, we conducted a permutational ANOVA ('adonis' using the R package 'vegan'[78]) based on Euclidean distance matrices using enzyme activity rates per unit soil C. Results are displayed in a non-metric multidimensional scaling plot.

Data availability. The soil carbon-related datasets generated and analysed during this study are available from the Powell Center soil carbon database and are available from the corresponding author upon request. All other data are included in this published article and its Supplementary Information files and no third-party data have been used.

References

43. *Guidelines for Soil Description* 4th edn (FAO, 2006).
44. IUSS Working Group WRB. *World Reference Base for Soil Resources 2014: Update 2015* World Soil Resources Reports 106 (FAO, 2015).
45. Harden, J. W. *Soils Developed in Granitic Alluvium near Merced, California* USGS Bulletin 1590–A (US Government Printing Office, 1987).
46. Harden, J. W. Genetic interpretations of elemental and chemical differences in a soil chronosequence, California. *Geoderma* **43**, 179–193 (1988).
47. Marchand D. E. & Allwardt, A. *Late Cenozoic Stratigraphic Units in Northeastern San Joaquin Valley, California* USGS Bulletin 170 (US Government Printing Office, 1981).
48. White, A. F. in *Chemical Weathering Rates of Silicate Minerals* Reviews in Mineralogy Vol. 31 (eds White, A. F. & Brantley, S. L.) 407–458 (Mineralogical Society of America, 1995).

49. White, A. F. et al. Chemical weathering rates of a soil chronosequence on granitic alluvium: III. Hydrochemical evolution and contemporary solute fluxes and rates. *Geochim. Cosmochim. Acta* **69**, 1975–1996 (2005).

50. Baisden, W. T. et al. A multiisotope C and N modeling analysis of soil organic matter turnover and transport as a function of soil depth in a California annual grassland soil chronosequence. *Global Biogeochem. Cycles* **16**, 1135 (2002).

51. Smith, G. I., Bischoff, J. L. & Bradbury, J. P. in *An 800,000-year Paleoclimatic Record from Core Ol-92: Owens Lake, Southeast California* GSA Special Paper Vol. 317 (eds Smith, G. I. & Bischoff, J. L.) 143–160 (Geological Society of America, 1997).

52. Rheis, M. et al. A half-million year record of palaeoclimate from the Lake Manix Core, Mojave Desert, California. *Palaeogeogr. Palaeoclimatol. Palaeoecol.* **365**, 11–37 (2012).

53. Paruleo, J. M., Epstein, H. E., Lauenroth, W. K. & Burke, I. C. ANPP estimates from NDVI for the central grassland region of the United States. *Ecology* **78**, 953–958 (1997).

54. Gorelick, N. et al. Google Earth Engine: planetary-scale geospatial analysis for everyone. *Remote Sens. Environ.* **202**, 18–27 (2018).

55. Berhe, A. A. Decomposition of organic substrates at eroding vs. depositional landform positions. *Plant Soil* **350**, 261–280 (2012).

56. Harden, J. W. An index of soil development from field descriptions: examples from a chronosequence in central California. *Geoderma* **28**, 1–28 (1982).

57. Beuselinck, L. et al. Grain-size analysis by laser diffractometry: comparison with the sieve-pipette method. *Catena* **32**, 193–208 (1998).

58. Miller, B. A. & Schaetzl, R. J. Precision of soil particle size analysis using laser diffractometry. *Soil Sci. Soc. Am. J.* **76**, 1719–1727 (2011).

59. Blake, G. R. & Hartge, K. H. in *Methods of Soil Analysis, Part I. Physical and Mineralogical Methods* Agronomy Monograph Vol. 9 (ed. Klute, A.) 363–375 (American Society of Agronomy—Soil Science Society of America, Madison, 1986).

60. Herbillon, A. J. Chemical estimation of weatherable minerals present in the diagnostic horizons of low activity clay soils. In: *Proc. 8th Int. Soil Classification Workshop* Part 1 (eds Beinroth, F. H., Camargo, M. N. & Eswaran, H.) 39–48 (EMBRAPA-SNLCS/SMSS/USDA-SCS/UPR, 1986).

61. Chao, T. T. & Sanzolone, R. F. Decomposition techniques. *J. Geochem. Explor.* **44**, 65–106 (1992).

62. Mehra, O. P. & Jackson, M. L. Iron oxide removal from soils and clays by a dithionite–citrate system buffered with sodium bicarbonate. *Clay Miner.* **5**, 317–327 (1960).

63. Hendershot, W. H, Lalande, H. & Duquette, M. in *Soil Sampling and Methods of Analysis* (ed. Carter, M. R.) 167–176 (Lewis Publishers, Boca Raton, 1993).

64. Robert, M. & Tessier, D. Méthode de préparation des argiles des sols pour des études minéralogiques. *Ann. Agron.* **25**, 859–882 (1974).

65. Brindley, G. W. & Brown, G. *Crystal Structures of Clay Minerals and Their Identification* Mineralogical Society Monograph 5 (Mineralogical Society, London, 1980).

66. Brunauer, S., Emmett, P. H. & Teller, E. Adsorption of gases in multimolecular layers. *J. Am. Chem. Soc.* **60**, 309–319 (1938).

67. Stewart, C. E., Paustian, K., Plante, A. F., Conant, R. T. & Six, J. Soil carbon saturation: linking concept and measurable carbon pools. *Soil Sci. Soc. Am. J.* **72**, 379–392 (2008).

68. Paul, E. A., Morris, S. J. & Boehm, S. in *Assessment Methods for Soil Carbon* Advances in Soil Science (eds Lal, R. et al.) 193–206 (CRC/Lewis Publishers, Boca Raton, 2001).

69. Xu, X. et al. Modifying a sealed tube zinc reduction method for preparation of AMS graphite targets: reducing background and attaining high precision. *Nucl. Instrum. Meth B* **259**, 320–329 (2007).

70. Stuiver, M. & Polach, H. A. Discussion reporting of ^{14}C data. *Radiocarbon* **19**, 355–363 (1977).

71. Bodé, S., Denef, K. & Boeckx, P. Development and evaluation of a high-performance liquid chromatography/isotope ratio mass spectrometry methodology for 13C analyses of amino sugars in soil. *Rapid Commun. Mass Spectrom.* **23**, 2519–2526 (2009).

72. Kaiser, C. et al. Belowground carbon allocation by trees drives seasonal patterns of extracellular enzyme activities by altering microbial community composition in a beech forest soil. *New Phytol.* **187**, 843–858 (2010).

73. Schindlbacher, A., Schnecker, J., Takriti, M., Borken, W. & Wanek, W. Microbial physologiy and soil CO_2 efflux after 9 years of soil warming in a temperate forest—no indications for thermal adaptions. *Global Change Biol.* **21**, 4265–4277 (2015).

74. Sinsabaugh, R. L. et al. Stichiometry of soil enzyme activtiy at global scale. *Ecol. Lett.* **11**, 1252–1264 (2008).

75. Lashermes, G., Gainvors-Claisse, A., Recous, S. & Bertrand, I. Enzymatic strategies and carbon use efficiency of a litter-decomposing fungus grown on maize leaves, stems, and roots. *Front. Microbiol.* **7**, 1315 (2016).

76. IBM Corp. IBM SPP Statistics for Windows. v.24.0 (IBM, 2016).

77. R Core Team. *R: A Language and Environment for Statistical Computing* (R Foundation for Statistical Computing, 2016); http://www.R-project.org/.

78. Oksanen, J. et al. vegan: Community Ecology Package. R Package v.2.4-3 (2017).